

Experimental images of heterogeneous turbid media by frequency-domain diffusing-photon tomography

M. A. O'Leary, D. A. Boas, B. Chance, and A. G. Yodh

Department of Physics and Department of Biochemistry and Biophysics, University of Pennsylvania, Philadelphia, Pennsylvania 19104

Received October 31, 1994

We present images of heterogeneous turbid media derived from measurements of diffuse photon-density waves traveling through highly scattering tissue phantoms. To our knowledge, the images are the first experimental reconstruction based on data collected in the frequency domain. We demonstrate images of both absorbing and scattering heterogeneities and show that this method is sensitive to the optical properties of the heterogeneity. The algorithm employs a differential measurement scheme that reduces the effect of errors resulting from incorrect estimation of the background optical properties. The relative advantages of sources with low and high modulation frequency are discussed within this context.

Near-infrared diffusing-light probes offer new possibilities for medical applications such as the non-invasive measurement of tissue oxygenation¹ in homogeneous tissues. Direct imaging of the optical properties of heterogeneous tissue is an important potential improvement to these schemes that has only recently been considered.^{2,3}

In this study we employ amplitude-modulated (frequency-domain) sources of photons that are injected into a scattering medium to generate diffuse photon-density waves⁴ (DPDW's). The diffusive waves are composed of randomly walking photons that collectively produce an exponentially damped spherical wave of photon density propagating outward from the source with well-defined amplitude and phase at each position in the medium. DPDW's have been shown to refract,⁵ diffract,^{4,6} disperse,⁷ scatter,⁸ and interfere.⁹ The contrast in images derived from these waves relies on intrinsic absorption or scattering variations within tissue or on similar variations generated by externally administered chromophores such as absorbing and fluorescing dyes.¹⁰

In this Letter measurements of the phase and amplitude of DPDW's are used to derive images of both single and multiple objects embedded within tissue phantoms. We experimentally demonstrate sensitivity to the optical properties of the objects and present images of pure scattering and pure absorbing inhomogeneities. To our knowledge, these demonstrations are the first experimentally derived images based on data collected in the frequency domain. The inversions utilize a perturbation expansion of the photon diffusion equation, and the experiments employ a simple differential measurement scheme designed to probe directly the perturbed part of the DPDW.

Several algorithms have been developed to model the forward problem for the diffusion of photons through heterogeneous media.^{2,3,11} In the limit in which spatial changes in absorption (μ_a) and scattering (μ_s') coefficients are small, each approach yields the same integral equation to first order in these

variations.¹² The standard perturbation expansion as described by Arridge *et al.*¹³ divides the absorption and diffusion coefficients $\{\mu_a, D = v/[3(\mu_a + \mu_s')]\}$ into spatially dependent $[\delta\mu_a(\mathbf{r}), \delta D(\mathbf{r})]$ and independent (background) (μ_a^o, D_o) pieces, i.e., $\mu_a(\mathbf{r}) \Rightarrow \mu_a^o + \delta\mu_a(\mathbf{r})$ and $D(\mathbf{r}) \Rightarrow D_o + \delta D(\mathbf{r})$. These terms are then incorporated into the diffusion equation, whose formal solution can be expressed as an integral equation by use of the appropriate Green function. In our case the light energy density is expanded in a perturbative series, i.e., $U(\mathbf{r}) = U_0(\mathbf{r}) + U_1(\mathbf{r}) + \dots$, and solved to first order. The first-order perturbative solution to the heterogeneous equation in the limit in which $U_1 \ll U_0$ is given by

$$U_0(\mathbf{r}_s, \mathbf{r}_d) = M \exp(ik_o|\mathbf{r}_s - \mathbf{r}_d|)/(4\pi D_o|\mathbf{r}_s - \mathbf{r}_d|), \quad (1)$$

$$U_1(\mathbf{r}_s, \mathbf{r}_d) = \int_V [-\delta\mu_a(\mathbf{r})vD_o^{-1}U_0(\mathbf{r}_s, \mathbf{r})G(\mathbf{r}, \mathbf{r}_d) + \frac{\delta D(\mathbf{r})}{D_o} \nabla U_0(\mathbf{r}_s, \mathbf{r}) \cdot \nabla G(\mathbf{r}, \mathbf{r}_d)] d^3r, \quad (2)$$

where M is the ac amplitude of a source located at \mathbf{r}_s , $G(\mathbf{r}, \mathbf{r}_d)$ is the Green function solution of the homogeneous equation at detector position \mathbf{r}_d , v is the speed of light in the medium, and $k_o = [(-v\mu_a^o + i\omega)/D_o]^{1/2}$ is the photon density wave number, where ω is the source modulation angular frequency. The Green function for an infinite medium is $G(\mathbf{r}, \mathbf{r}_d) = \exp(ik_o|\mathbf{r} - \mathbf{r}_d|)/(4\pi|\mathbf{r} - \mathbf{r}_d|)$. The integral is over the entire sample volume. For absorbing inhomogeneities the first term in Eq. (2) was used in the reconstruction, and for purely scattering inhomogeneities the second term was used, i.e., $\delta D/D_o = \delta\mu_s'/(\mu_a^o + \mu_s'^o + \delta\mu_s'^o)$, with $\delta\mu_a = 0$. We have also investigated other perturbation schemes¹⁴ that place different restrictions on absorption variation, and they yielded qualitatively similar results to those presented here.

For the image reconstruction the integral equation (2) is digitized into a sum over voxels, and the amplitude and phase of the DPDW are measured

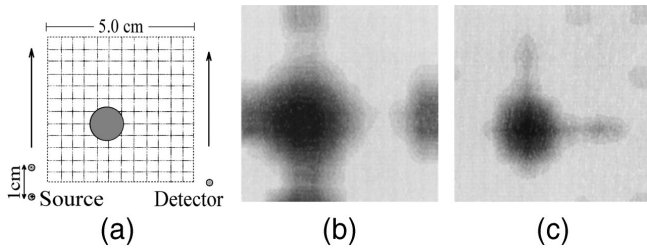


Fig. 1. (a) Experimental geometry with the actual position of a 1.2-cm-diameter sphere and the reconstruction of (b) a perfectly absorbing sphere and (c) a highly scattering sphere. Both reconstructions were generated by use of 1000 iterations of the simultaneous iterative technique.

in different source–detector configurations. This yields a set of coupled linear equations that relates the real and imaginary parts of the measurements to the values of μ_a and μ_s' in the various voxels within the sample. There are many methods available to find the best solution to the inverse problem; however, care must be taken since the integral equation is a Fredholm integral of the first kind and is highly susceptible to high-frequency noise. For our reconstructions we have used two techniques: (1) an algebraic technique called the simultaneous iterative technique with constraints¹⁵ and (2) a regularized matrix inversion based on singular-value decomposition and analysis.¹⁶ In our reconstructions using the first technique we have constrained the reconstructed absorption to be greater than zero, and the number of iterations is a free parameter. In the matrix inversion we use variable smoothing to reduce high-frequency noise in the singular values.

Our experimental apparatus was described previously.⁵ Briefly, our setup consists of a large glass tank (40 L) filled with a model turbid biological material called Intralipid. Typically an amplitude-modulated (220-MHz) laser diode (~ 3 mW, 780 nm) is fiber coupled into the medium, and a second fiber is used to detect diffuse photon-density waves as a function of position within the tank. Using standard heterodyne techniques, we determine the phase and amplitude of the diffuse photon-density waves in the medium. Figure 1(a) shows the measurement geometry. A single measurement consists of subtracting the signal obtained from two sources equidistant from the detector. Since the signal we measure is a sum of the incident wave and the perturbed wave, the subtraction cancels the unperturbed signal [$U_o(\mathbf{r})$], leaving only the signal that is due to the perturbation [$U_1(\mathbf{r})$]. Equations (1) and (2) are then simply modified to include two sources rather than one.¹⁷ This subtraction becomes critical when the background properties of the medium are not well known.

The initial amplitude and phase of the sources were measured for calibration purposes, and then the objects (black wooden balls for perfect absorbers and resin spheres containing titanium oxide and ink¹⁸) were submerged and moved in a manner to simulate the source pair scanning along the sides of a 6.0 cm \times 6.0 cm square. In each measurement the detector remained directly opposite the source pair at a separation of greater than 35 transport mean free

paths. Approximately 120 measurements of amplitude and phase were made around the square. The volume of the imaged region was ≈ 36 cm³.

Figures 1(b) and 1(c) demonstrate the reconstruction of a single spherical object (1.2 cm in diameter) from experimental data. The background medium has $\mu_a^o = 0.023$ cm⁻¹ and $\mu_s'^o = 6.0$ cm⁻¹. In Fig. 1(b) a single perfectly absorbing inhomogeneity is imaged, and in Fig. 1(c) a resin sphere having the same absorption coefficient as the surrounding medium but a higher scattering coefficient ($\mu_s' \approx 15.0$ cm⁻¹) is imaged. In each reconstruction we have made use of *a priori* knowledge that the object is either absorbing or scattering.

To confirm that the method is sensitive to the optical properties of the medium, we carried out a series of experiments in which spheres of varying absorption were imaged separately, using matrix inversion (singular-value decomposition). The reconstructed $\delta\mu_a(\mathbf{r})$ for both the experimental data and the simulated data (generated by use of the exact solution) is shown in Fig. 2. Note that the reconstructed absorption (filled circles) qualitatively follows the actual object absorption but saturates at large absorption, where perturbation theory is expected to break down. The noise-reducing filter used in the singular-value analysis has the effect of reducing the magnitude of the reconstructed $\delta\mu_a(\mathbf{r})$, so all reconstructed values have been multiplied by 2. We found that the reconstructed values of $\delta\mu_a(\mathbf{r})$ are offset by a small additive constant, as a result of the mismatch of both index of refraction and reduced scattering coefficient between the resin sphere and Intralipid.

Figures 3(a) and 3(b) experimentally demonstrate that we are able to resolve multiple absorbing objects. We have also investigated the effect of modulation frequency on the resolution of multiple objects, using simulated data derived from the analytic solution for a sphere.⁸ The simulations in Figs. 3(c)–3(f) demonstrate that, when the background absorption is high ($\mu_a = 1.0$ cm⁻¹), an increase in the modula-

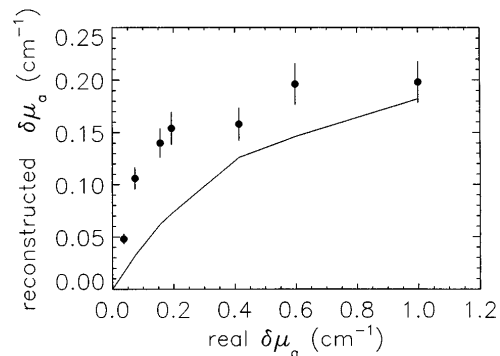


Fig. 2. Reconstructed absorption from both the experimental data (filled circles) and the simulated data (solid curve) versus the actual absorption. In this experiment, resin spheres (1.2 cm in diameter) made with a mixture of scatterer and a known concentration of ink were imaged by matrix inversion. The error bars are derived from estimating the calibration errors that we believe to be most significant.

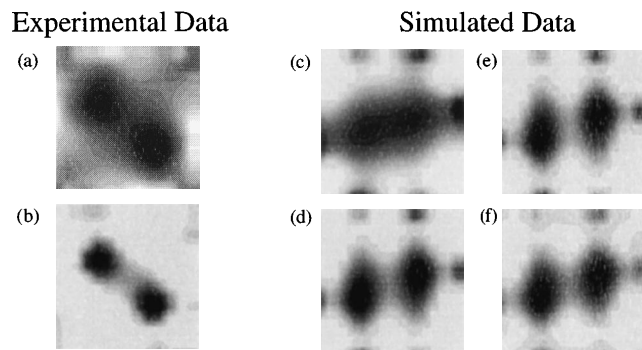


Fig. 3. Reconstruction of two 1.0-cm-diameter perfectly absorbing spheres from experimental data, using (a) singular-value decomposition and analysis and (b) 3000 iterations of the simultaneous iterative technique. (c)–(f) Images of two perfectly absorbing spheres from simulated data, using a different sphere configuration. In (c) and (d) (background $\mu_a = 0.1 \text{ cm}^{-1}$, inside the spheres $\mu_a = 0.4 \text{ cm}^{-1}$) we see an increase in image quality as the modulation frequency is increased from (c) 50 MHz to (d) 1 GHz. However, when the background absorption is high (background $\mu_a = 1.0 \text{ cm}^{-1}$, inside the spheres $\mu_a = 4.0 \text{ cm}^{-1}$) the image quality does not noticeably improve as the modulation frequency is increased from (e) 50 MHz to (f) 1 GHz.

tion frequency from 50 MHz to 1 GHz has little or no effect on the image quality. We do, however, observe a modulation-frequency-dependent improvement in image quality in systems with a low background absorption (i.e., $0.01 \text{ cm}^{-1} < \mu_a < 0.1 \text{ cm}^{-1}$). We may understand this qualitatively by noting that the wave number of a DPDW, $k = [(-v\mu_a + i\omega)/D]^{1/2}$, is nearly independent of ω when $v\mu_a \gg \omega$. This result suggests that sources at low modulation frequencies and sources with high-frequency components will yield roughly equivalent images in media that are characterized by a high average absorption, such as the brain. On the other hand, for imaging within bodies with low average absorption, such as the breast, high-modulation-frequency images will give better resolution.

In conclusion, we have used diffuse photon-density waves to obtain experimentally images of highly scattering tissue phantoms. The image reconstruction approach can be easily extended to encompass pulsed (time-domain) sources by summation over the DPDW's that compose the pulse train.

It is a pleasure to acknowledge conversations with Jolyon Browne, Michael Glazov, Michael Cohen, Dinos Gonatas, and John Schotland. A. G. Yodh acknowledges partial support through the Presidential Young Investigator program, grant NSF-DMR-9003687, and from the Alfred P. Sloan Foundation. B. Chance acknowledges support in part by National Institutes of Health grants NS-27346, HL-44125, and CA-50766/60182.

References

1. M. Tamura, O. Hazeki, S. Nioka, and B. Chance, *Annu. Rev. Physiol.* **51**, 813 (1989).
2. See related studies in R. R. Alfano, ed., *Advances in Optical Imaging and Photon Migration*, Vol. 21 of OSA Proceedings Series (Optical Society of America, Washington, D.C., 1994).
3. See related studies in G. Muller, ed., *Medical Optical Tomography: Functional Imaging and Monitoring* (Society of Photo-Optical Instrumentation Engineers, Bellingham, Wash., 1993), Vol. Is11, p. 31.
4. J. B. Fishkin and E. Gratton, *J. Opt. Soc. Am. A* **10**, 127 (1993).
5. M. A. O'Leary, D. A. Boas, B. Chance, and A. G. Yodh, *Phys. Rev. Lett.* **69**, 2658 (1992).
6. D. A. Boas, M. A. O'Leary, B. Chance, and A. G. Yodh, *Phys. Rev. E* **47**, R2999 (1993).
7. B. J. Tromberg, L. O. Svaasand, T. T. Tsay, and R. C. Haskell, *Appl. Opt.* **32**, 607 (1993).
8. D. A. Boas, M. A. O'Leary, B. Chance, and A. G. Yodh, *Proc. Natl. Acad. Sci. USA* **91**, 4887 (1994).
9. J. M. Schmitt, A. Knüttel, and J. R. Knutson, *J. Opt. Soc. Am. A* **9**, 1832 (1992); B. Chance, K. Kang, L. He, J. Weng, and E. Sevick, *Proc. Natl. Acad. Sci. USA* **90**, 3423 (1993).
10. M. A. O'Leary, D. A. Boas, B. Chance, and A. G. Yodh, *J. Lumin.* **60–61**, 281 (1994).
11. We are aware of a prior unpublished study by J. Schotland, J. S. Leigh, M. Ishii, and C. P. Gonatas (Department of Radiology, University of Pennsylvania, Philadelphia, Pa.) on the inverse problem with diffusing photons. In particular, these authors present a method for direct inversion of the data whose kernel, which is calculated within a one-loop diagrammatic approximation, is accurate to all orders in variation of $\mu_a(\mathbf{r})$ and $D(\mathbf{r})$.
12. The condition that $\delta\mu_a \ll \mu_a$ and $\delta\mu_s' \ll \mu_s'$ is sufficient to reduce each solution to an integral equation linear in $\delta\mu_a$ and $\delta\mu_s'$.
13. S. R. Arridge, P. van der Zee, M. Cope, and D. T. Delpy, *Proc. Soc. Photo-Opt. Instrum. Eng.* **1431**, 204 (1991).
14. In the Rytov formulation¹⁵ the heterogeneous photon-density wave is expressed as the homogeneous wave with a complex phase shift (ϕ) owing to the perturbation, i.e., $U = U_o \exp(\phi)$ and $\phi = [1/U_o(\mathbf{r}_s, \mathbf{r}_d)] \int_V [-\delta\mu_a(\mathbf{r})vD_o^{-1}U_o(\mathbf{r}_s, \mathbf{r})G(\mathbf{r}, \mathbf{r}_d) + \delta D(\mathbf{r})/D_o \nabla U_o(\mathbf{r}_s, \mathbf{r}) \cdot \nabla G(\mathbf{r}, \mathbf{r}_d)] d^3r$. In general, the first Rytov approximation is valid when $(\nabla\phi)^2 \ll v\delta\mu_a/D$.
15. A. C. Kak and M. Slaney, *Principles of Computerized Tomographic Imaging* (Institute of Electrical and Electronics Engineers, New York, 1988), Chap. 6, p. 211.
16. W. H. Press, B. P. Flannery, S. A. Teukolsky, and W. T. Vetterling, *Numerical Recipes in C: The Art of Scientific Computing* (Cambridge U. Press, New York, 1988), Chap. 2, p. 52. The singular values ω_i are put through the following filter: $\omega_i \rightarrow \omega_i + \sigma/\omega_i$, where the amount of smoothing, σ , is a free parameter.
17. To incorporate two sources, one simply replaces $U_o(\mathbf{r}_s, \mathbf{r})$ by $U_o(\mathbf{r}_{s1}, \mathbf{r}) - U_o(\mathbf{r}_{s2}, \mathbf{r})$ in Eq. (2).
18. M. Firbank, M. Hiraoka, and D. Delpy, *Phys. Med. Biol.* **38**, 847 (1993).